Designing organic spin filters in the coherent tunneling regime

Carmen Herrmann,[1,a)] Gemma C. Solomon,[2] and Mark A. Ratner[1]
[1]*Department of Chemistry, Northwestern University, 2145 Sheridan Road, Evanston, Illinois 60208-3113, USA*
[2]*Nano-Science Center and Department of Chemistry, University of Copenhagen, Universitetsparken 5, Copenhagen Ø, 2100 Denmark*

(Received 19 November 2010; accepted 19 May 2011; published online 13 June 2011)

Spin filters, that is, systems which preferentially transport electrons of a certain spin orientation, are an important element for spintronic schemes and in chemical and biological instances of spin-selective electronic communication. We study the relation between molecular structure and spin filtering functionality employing a theoretical analysis of both model and stable organic radicals based on substituted benzene, which are bound to gold electrodes, with a combination of density functional theory and the Landauer–Imry–Büttiker approach. We compare the spatial distribution of the spin density and of the frontier central subsystem molecular orbitals, and local contributions to the transmission. Our results suggest that the delocalization of the singly occupied molecular orbital and of the spin density onto the benzene ring connected to the electrodes, is a good, although not the sole indicator of spin filtering functionality. The stable radicals under study do not effectively act as spin filters, while the model phenoxy-based radicals are effective due to their much larger spin delocalization. These conclusions may also be of interest for electron transfer experiments in electron donor–bridge–acceptor complexes. © *2011 American Institute of Physics*. [doi:10.1063/1.3598519]

I. INTRODUCTION

Organic spintronics is of interest due to its potential for combining the advantages of spintronics,[1–3] such as low-power operation, and organic electronics, in particular flexibility and low fabrication cost.[4–6] While in most cases, inherently nonmagnetic organic layers are employed, building the ferromagnetic parts of the system from organic components has also been proposed,[7,8] for example, from organic radicals packed in a crystal[9] or from polymers with radical subunits.[10,11] Such components may in principle act as spin filters, that is, as building blocks which preferentially transport electrons of a certain spin orientation. Here, we focus on the spin filtering capabilities of the molecular subunits of such magnets.

Spin filtering requires control over the orientation of the spin polarization of the molecular subunit with respect to the spin of the transported electrons. Ideally, this control would be absolute, for example, through external fields. Spin filtering could also play a role when only the relative orientation of transported spins and the filtering molecule can be controlled: It is possible to imagine having molecular spin filters connected in a way that makes both parallel and antiparallel alignment of their spins energetically accessible, and thus may result in a switch for overall charge transport which can be operated by changing the spin coupling. This functionality may be rationalized in part by assuming that each subunit transports preferentially electrons of one spin, depending on its own spin orientation, and that by switching the relative spin orientation of adjacent subunits, part of the electrons let through by one can be blocked by the other. A first step to understand the behavior of these composite systems is to study the molecular subunits. In a second step it will be necessary to study to which extent the behavior of the larger aggregates can be explained in terms of the behavior of the subunits.

To understand the spin filtering properties that are due to single molecules, it makes sense to examine them in a variety of environments and to identify unique properties by comparison. Experimentally, organic radical bridges have been studied using conductance measurements on gold nanoparticle arrays, where radicals bridge the nanoparticles,[12] and in electron donor–bridge–acceptor complexes.[13,14] For the latter, it has been found that radical bridges may influence the charge recombination dynamics of the charge separated state, and that these dynamics depend on the spin state of the charge-separated system.

While modeling electron transfer rates accurately can be a challenge, it may be possible for certain systems to obtain a qualitative picture of the bridge's contribution to charge transfer from coherent tunneling calculations within the Landauer–Imry–Büttiker approximation[15,16] in combination with a Green's function approach[17] and Kohn–Sham density functional theory (KS-DFT),[18] with the molecule sandwiched between gold electrodes. This approach allows various electron injection energies to be sampled, providing results which may be relevant for a variety of donor and acceptor systems and also for metal junction setups that are dominated by coherent tunneling. It has been applied predominantly to closed-shell structures, but in recent years, open-shell molecular bridges have been investigated.[19–27]

When designing spin filters, it would be advantageous to have some general rules predicting their filtering capability based on their chemical structure rather than having to carry

a)Author to whom correspondence should be addressed. Electronic mail: carmen.herrmann@chemie.uni-hamburg.de. TEL.:+49-40-42838-6934. FAX.: +49-40-42838-2882. Present address: Department of Chemistry, University of Hamburg, Martin-Luther-King-Platz 6, 20146 Hamburg, Germany.

out a transport calculation for each candidate. This would also allow for established rules of thumb for the relation between chemical structure and electronic structure of organic radicals to be exploited.[28] We take a closer look here at how spin filtering behavior may be estimated from the shape and energetics of the frontier molecular orbitals (MOs), which of course also control the spin density. Intuitively, we anticipate that the spin density distribution, which within an effective single-particle model such as KS-DFT is determined by the MO shapes and energies, plays a decisive role. To fully exploit the capabilities of synthetic chemistry for designing spin filters, it would be helpful to have a more detailed picture. Furthermore we show, by studying local (atomic) contributions to the transmission, which parts of the molecular structure contribute to the dips and peaks in the transmission of benzene-based systems that occur due to the radical substituent.

The combination of Landauer–Imry–Büttiker approach, Green's function techniques, and KS-DFT has been described in numerous publications[29–33] and shall therefore only be summarized briefly. The junction is usually separated into the two semi-infinite electrodes, and into a central region (or subsystem), which may comprise the molecule or the molecule and part of the electrodes. The electronic structure of the central region is described using an effective one-particle model such as KS-DFT or Hartree–Fock theory. By solving the secular equation for the central region only, a set of one-electron levels is obtained (central subsystem molecular orbitals, CMOs). Assuming that electron transport is a coherent tunneling process, that the electrodes are reflectionless, that a steady state is reached, and that the voltage division is symmetric,[34,35] the current of electrons of spin $\sigma \in \{\alpha, \beta\}$ at a temperature of 0 K can be expressed as

$$I_\sigma = \frac{e}{h} \int_{E_F - \frac{eV}{2}}^{E_F + \frac{eV}{2}} dE T_\sigma(E, V), \tag{1}$$

where e is the magnitude of the electron charge, h Planck's constant, E_F the Fermi energy of the electrodes in equilibrium (assuming that the two electrodes are equivalent), and T_σ is the spin-dependent transmission which depends on the energy E of the tunneling electron and on the bias voltage V. Within the Landauer–Imry–Büttiker approximation, the zero-voltage conductance $(dI/dV)_{V=0}$ is proportional to $T(E_F)$. The transmission can be calculated[36,37] as the trace over the matrix product of the coupling matrices $\mathbf{\Gamma}_{R/L,\sigma}$ for the left and right electrode, and the advanced and retarded Green's function of the central region $\mathbf{G}^{r/a}_{C,\sigma}$ (with $\mathbf{G}^{a}_{C,\sigma} = (\mathbf{G}^{r}_{C,\sigma})^\dagger$),

$$T_\sigma(E, V) = tr(\mathbf{\Gamma}_{R,\sigma} \mathbf{G}^{r}_{C,\sigma} \mathbf{\Gamma}_{L,\sigma} \mathbf{G}^{a}_{C,\sigma}). \tag{2}$$

The Green's functions and coupling matrices have been obtained by postprocessing the one-particle Hamiltonian and overlap matrices obtained for molecules attached to finite-size gold clusters mimicking the electrodes (see Appendix A for further details). Since the transmission may be interpreted as a measure of an electron's propensity to tunnel through the junction, we judge the spin filtering properties of a bridge from whether α (majority spin) and β (minority spin) transmission differ over a significantly broad energy range. Spin–orbit coupling is neglected, and current-induced spin flips, inelastic changes of spin states, vibrational excitations, and temperature effects are not considered in this initial study.

We decompose the transmission into local contributions[38–40] as outlined in Ref. 40,

$$T(E) = \sum_{A \in M_L, B \in M_R} T_{AB}(E), \tag{3}$$

where $T_{AB}(E)$ is the transmission between centers A and B. In the following, A and B are atoms belonging to two sets M_L and M_R which are to the left and right of some interface of interest. Further, A and B are defined by the basis functions centered on them after a symmetric (Löwdin) orthogonalization.

It should be stressed that we are interested in spin filtering in a general sense here, which may include different forms of spin-dependent electronic communication through radical bridges, and the chosen molecular junction setup is a convenient tool to do so rather than a practical suggestion for a spin filtering device. Also, the proper choice of the Fermi energy is a question that has not been completely resolved yet, and for practical purposes, a range of values may be considered reasonable. Therefore, we have not included plots of spin-polarized currents and current ratios here. Such plots may be found for structures **1** and **2** in the Supporting Information of Ref. 24.

After introducing the systems and comparing their spin-resolved transmission in Sec. II, we study the influence of density functional and basis set on the transmission in Sec. III. The local transmission, molecular orbitals and spin density are discussed in Sec. IV. Finally, Sec. V summarizes the results and provides an outlook on future research directions. Details on the computational methodology are given in Appendix A. The supplementary material[41] provides additional data on molecular orbitals, parameter dependence, and local transmission.

II. SPIN-RESOLVED TRANSMISSION

Here, we compare several organic radicals to identify rules for what makes a radical a good spin filter. Two of these are model phenoxy radicals, benzene rings connected to the electrodes via C≡CS linkers either *para* or *meta* to one another, with an oxygen radical substituent (structures **1** and **2** in Figure 1). Their spin filtering behavior has been studied previously by computation,[24] and they were found to have a large difference between α and β transmission. We compare these model radicals with two stable *meta*-connected benzene bridges with a nitronyl nitroxide (structure **3**) or *t*-butylphenylnitroxide (structure **4**) group attached; these turn out to show only little difference between the transmission for the two spin orientations (see Figure 1). For comparison, we also look at the hydroxy analog of **4**, as investigated in Ref. 14 (structure **5**). Systems **1** to **4** are investigated in their doublet state. The central region consists of the molecule only, if not mentioned otherwise.

Figure 1 shows the transmission for α (majority spin) and β (minority spin) electrons for the five systems under study here, calculated with the B3LYP density functional[42,43] and

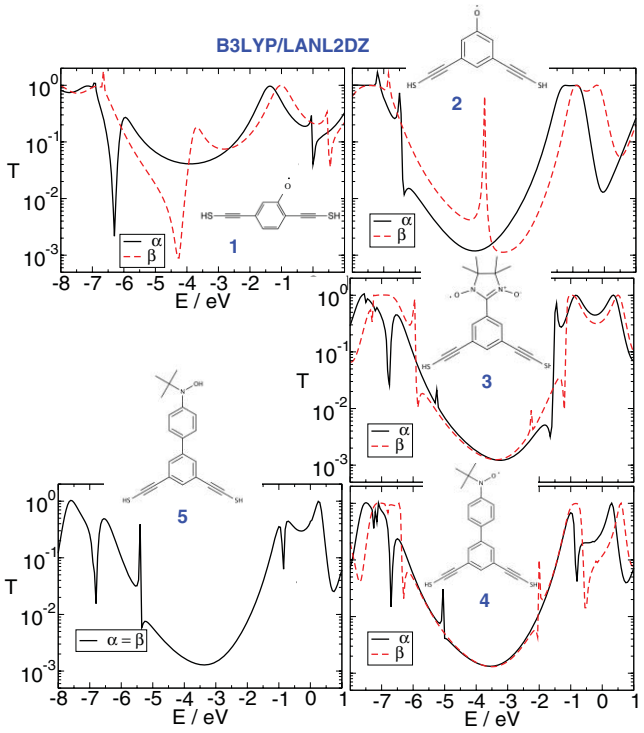

FIG. 1. Spin-resolved transmission calculated for α (majority spin, black curves) and β (minority spin, dotted red curves) electrons. The data for **1** and **2** have already been presented in different form in Ref. 24 and are included here for comparison. While the differences between α and β transmission are considerable for **1** and **2**, they are minor for **3** and **4**.

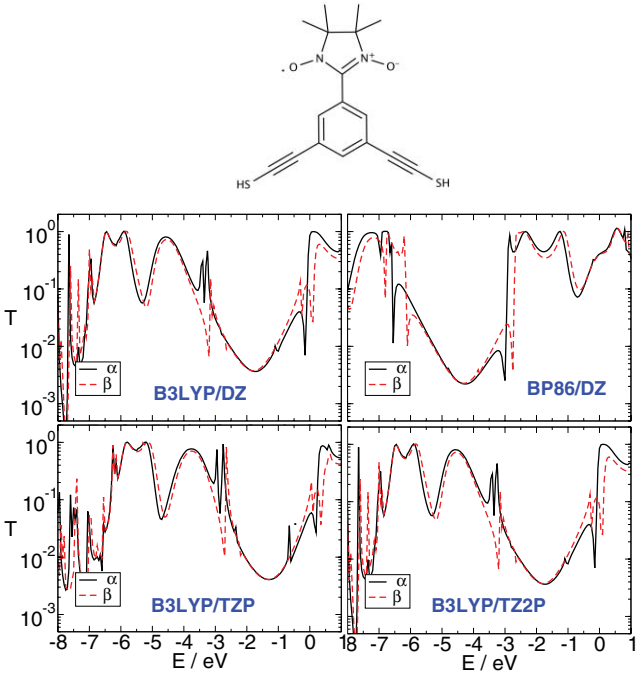

FIG. 2. Spin-resolved transmission calculated with various functionals and basis sets for **3**. While the details of the transmission curves vary with the functional and basis set, qualitative conclusions (such as the overall similar transmission for α and β electrons in this case) are not affected by this choice.

the effective core potential LANL2DZ with matching double-zeta basis set.[44]

We are mostly interested in the energy range around the HOMO-LUMO (highest occupied and lowest unoccupied molecular orbital) gaps which is approximately between −1 and −7 eV for the systems studied here using B3LYP (see Sec. IV A). While the appropriate choice of the Fermi energy is an unsolved problem which makes quantitative predictions of current–voltage curves difficult,[45] this energy range includes all reasonable choices for the Fermi energy of gold electrodes. It may also be expected to include the energetic range accessible by electron transfer experiments. We examine only the elastic scattering limit, ignoring concerns about the relation between molecular resonances and the gold Fermi energy and the potentially increasing importance of vibrational contributions when these are close in energy.[46]

All transmission curves in Figure 1 can be described as composed from a smooth "baseline," which resembles the transmission of the analogous unsubstituted benzene systems,[40] and peaks or dips which are caused by the radical substituent acting as an additional site in the π-electron system. As discussed in Ref. 24, the qualitative shape of these curves can be explained by a simple Hückel model describing the π electron system. The "baseline" of all transmission curves looks as expected for *para*- and *meta*-connected benzene systems: for the former (system **1**), the baseline is higher by more than an order of magnitude over a broad energy range than for the latter (systems **2** to **5**). The peaks in the transmission of systems **2** to **5** are often accompanied by (smaller) dips and could therefore be more accurately described as a Fano resonance. Fano resonances have been studied previously in the context of molecular electronics.[47,48] Due to the variability of lineshapes with the density functional chosen (see Figure 2 below), and since their detailed form is not essential for spin filtering, we are not discussing them in depth here.

For the oxygen-substituted radicals **1** and **2**, there are broad dips and peaks, respectively, in the transmission, which are shifted by about 2 eV to higher energies when comparing β to α transmission. Additionally, the "baseline" is shifted to higher energies by 0.5 to 1 eV for the β curve compared with the α one.

For the stable radicals **3** and **4**, the differences between α and β transmission are much smaller: The peaks and dips are considerably narrower, and the α and β baselines are only barely shifted for **3** and coincide for **4** in the energy range of main interest here. This suggests that any differences in charge recombination rates between the singlet and triplet charge separated states as observed in Refs. 13 and 14 are not due to the tunneling electron transport properties of the bridge. The α transmission of **4** is very similar to the transmission of its closed-shell counterpart **5**.

Since the current is obtained by integrating the transmission (Eq. (1)), adding a radical group or another substituent that participates in the π-electron system can diminish the differences in the transmission and thus in the conductivity between *para*- and *meta*-connected benzene systems by adding transmission dips to the former and peaks to the latter.

III. INFLUENCE OF DENSITY FUNCTIONAL AND BASIS SET ON THE SPIN-RESOLVED TRANSMISSION

Comparing the transmission obtained for **3** with different density functionals and basis sets (see Figure 2) illustrates why it is not advisable to interpret the small peaks and dips in too much detail: Depending on the choice of computational parameters, the location and shape of these peaks and dips can change considerably. For example, the B3LYP α transmission for **3** has a double peak to the left of the overall minimum (around −3 eV), whereas the whole curve is shifted to lower energies when using BP86, and the feature to the left of the minimum is now a dip. But the qualitative conclusions as to whether a molecular bridge acts as a spin filter are not affected by the choice of functional and basis set: From all graphs in Figure 2 one can conclude that **3** effectively does not act as a spin filter. The same is true for **4** (see supplementary material[41]). Accordingly, the parameter study presented in Ref. 24 suggests that **1** and **2** are good spin filters, irrespective of which parameters are chosen.

Surprisingly, the B3LYP/DZ results are quantitatively different from the B3LYP/LANL2DZ ones, although in both cases the basis set is of double-zeta quality and the same density functional is employed. This may be because while the B3LYP/LANL2DZ data in Figure 1 were obtained by post-processing electronic structure calculations carried out with the QCHEM program package[49] and effective core potentials[44] for the gold atoms in combination with Gaussian basis functions, the data presented in Figure 2 and Figure S3 in the supplementary material[41] come from all-electron calculations employing ADF (Ref. 50) in which Slater-type basis functions are used, and where the relativistic effects were described by the zeroth-order regular approximation.[51–53]

For this work, elucidating the relation between electronic structure and spin filtering properties, the parameter dependence is not crucial, since we want to see how electronic structure and spin filtering are related to each other from a general point of view. For more quantitative discussions, however, this parameter dependence should be kept in mind.

IV. LOCAL TRANSMISSION AND MOLECULAR ORBITALS

We now ask what makes a molecule a good spin filter. When comparing α and β transmission for a given structure, two phenomena may lead to substantial differences between the two curves and may thus be exploited for spin filtering: (1) shifts of the α and β transmission baselines with respect to each other, and (2) different shapes and shifts of the relative position of peaks or dips with respect to the baseline for different spins. Since to calculate conduction, a range of energies will be important, the latter mechanism may be expected to work only when the dips or peaks are sufficiently broad. Shifts of the baseline (accompanied by peak shifts) are exemplified in the transmission curves of **1** and **2** (top two panels in Figure 1), while shifts of the relative position of the peaks only can be seen for **3** and **4** (middle and lower right panel in Figure 1).

Within the KS-DFT-based Landauer–Imry–Büttiker methodology we are using here, transmission is determined by the energies and the shapes of the molecular orbitals obtained by solving the secular equation within the central region (the CMOs). In particular, peaks in the transmission are often found close to CMO energies. However, it is possible for several CMOs to interact, and for effects such as destructive interference[54–58] to lead to dips in the transmission. The peaks may be shifted in energy with respect to the CMO energies. As shown below, the energetic location of the "radical" peaks (and to a certain extent also of the dips) for our systems is typically very close to the CMO energies. There is then a clear relation between peak broadening and CMO contributions on the benzene ring directly connected to the electrodes. Thus, a CMO analysis can give valuable insight into the connection of electronic structure and spin filtering behavior.

Additionally, there are questions which a study of the shape and energies of the CMOs alone cannot answer, such as to what extent the tunneling electrons go through the radical substituent as opposed to through the benzene ring only. To this purpose, an analysis of local contributions to the transmission is helpful. In the following, the CMOs and local transmission (using B3LYP/LANL2DZ) are analyzed in more detail.

A. Central subsystem MOs and spin density

The energies of the frontier CMOs (in the following referred to as HOMO$^\alpha$, LUMO$^\alpha$, and so on) and isosurfaces of the spin density and the HOMO$^\alpha$ and the LUMO$^\beta$ of radicals **1** to **4** are given in Figure 3. The orbital occupation has been assigned by comparing the shapes of the CMOs to the MOs in the corresponding free radicals. The CMOs of **3** and **4** which are energetically located below and above the HOMO$^\alpha$/LUMO$^\beta$ can be found in the supplementary material,[41] and for **1** and **2** in Ref. 24 (reproduced here for comparison).

For all systems under study, the pairs of α and β CMOs with the same occupation number, HOMO-1$^\alpha$/HOMO$^\beta$ and LUMO$^\alpha$/LUMO+1$^\beta$, have similar energy, and the LUMO$^\beta$ is higher in energy by 2 to 3 eV than the HOMO$^\alpha$. For **4** the HOMO-1$^\alpha$/HOMO$^\beta$ and LUMO$^\alpha$/LUMO+1$^\beta$ pairs are very close in energy, they are slightly shifted for **1** to **3**, with the β CMOs having higher energies. This is reflected in a shift of the β transmission baseline to higher energies when compared with the α one (see Figure 1). For **4**, the two baselines virtually coincide over a broad energy range. What the CMO energy shifts cannot explain is why the baselines are shifted by up to 1 eV for **1** and **2**, whereas the shift is close to negligible for **3**.

The CMOs provide a good explanation for the width of the peaks and dips: Systems **1** and **2** have considerable contributions to the HOMO$^\alpha$/LUMO$^\beta$ and to the spin density from the benzene ring which is directly connected to the electrodes. For **3** and **4**, however, these contributions are negligible. Larger CMO contributions on the ring (in particular on atoms connected to the electrodes) will in

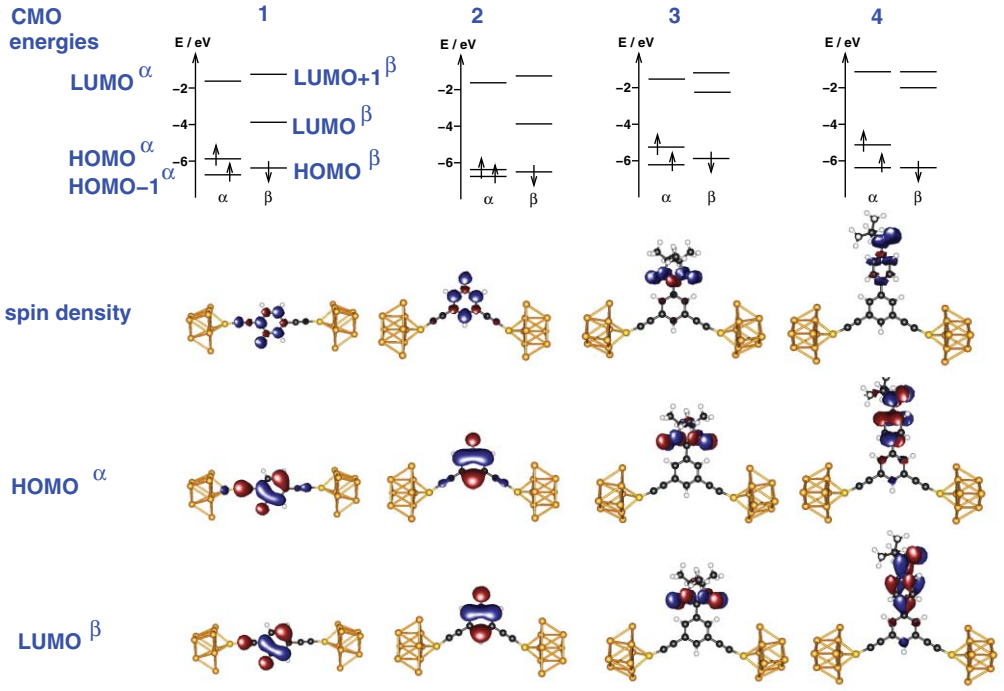

FIG. 3. Central subsystem MO energies (top), isosurface plots for α (third row) and β CMOs (fourth row), and total system spin density (second row). B3LYP/LANL2DZ.

general lead to larger coupling of the one-particle levels to the electrodes (from the coupling matrices $\mathbf{\Gamma}_{L/R,s}$ in Eq. (2)), and thus to broader transmission peaks. Indeed, the peaks close to the HOMO$^{\alpha}$/LUMO$^{\beta}$ energies (see Table I and Figure 1) are much broader for **2** than for **3** and **4**.

The dips in **1** are also very broad, although the relation between those dips and the CMOs is less straightforward to make. Interestingly, while **3** has more spin density on the ring than **4**, it has smaller HOMO$^{\alpha}$/LUMO$^{\beta}$ coefficients on the ring. This seems counterintuitive, but may be attributed to larger differences in shape (reflected in larger differences in energy) between α and β CMOs in **3**, so that not only the HOMO$^{\alpha}$/LUMO$^{\beta}$ is decisive for the spin density. Given the variability of the electronic structure and thus transmission with the computational parameters illustrated in Sec. III, it seems inadvisable to interpret these rather minor differences in much detail. Spin delocalization will depend strongly on the dihedral angle between the two rings in **3** and **4**; while **3** has a dihedral angle of 24.2° (B3LYP/TZVP optimized structure), **4** is more twisted, with a dihedral angle of 43.5° (B3LYP/TZVP) or 32.8° (BP86/TZVP).

The energies of the HOMO$^{\alpha}$ and LUMO$^{\beta}$ in the *meta*-connected systems **2** to **4** are very close to the position of the peaks which the transmission curves show on top of the baseline (see Table I). On the other hand, the position of the dips in system **1** is shifted by 0.4 eV to higher energies compared with the CMO energies.

TABLE I. Energies of the "radical" peak or dip in the α and β transmission for the four radicals under study, compared with the CMO energy corresponding to the HOMO$^{\alpha}$/LUMO$^{\beta}$. B3LYP/LANL2DZ.

		E(peak/dip)/eV	E(HOMO$^{\alpha}$/LUMO$^{\beta}$)/eV
1	α	−6.3	−5.9
	β	−4.3	−3.8
2	α	−6.5	−6.4
	β	−3.8	−3.8
3	α	−5.3	−5.2
	β	−2.3	−2.2
4	α	−5.1	−5.1
	β	−2.0	−2.0

B. Local transmission

An analysis of atomic contributions to the transmission[38–40,48] shows which parts of the molecular structure are directly participating in charge and spin transport. Previously,[40,48,59] analysis of the unsubstituted *meta* benzene systems revealed that the dips in the transmission associated with interference features were characterized by ring current reversal, while the unsubstituted *para* system has none of these features. In the substituted systems, **1** and **2**, the transmission reveals a number of interference features in each case. In the case of the α spin transport through **1**, the ring current reversal is evident around the interference feature induced by the radical substituent as shown in Figure 4. While it is not so simple to see the ring current reversal in the total transmission in other cases, as residual σ transport dominates near the interference features, a simple Hückel model for the π system in these molecules reproduces the transmission features and highlights the nature of the ring current reversals around the interference features. Detailed

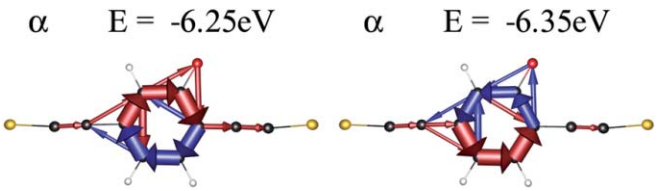

FIG. 4. The ring current reversal evident around the interference feature induced by the radical substituent in the α transmission (B3LYP/LANL2DZ). The diameter of an arrow between two atoms is proportional to the local transmission value between the atoms. Contributions below 10% of the largest local transmission value have been omitted. Arrows in transport direction are shaded red, and the ones opposite to it in blue. The apparent lack of conservation arises as Au - molecule terms are not shown in this plot.

local transmission plots for structures **1**, **2**, and **3** are given in the supplementary material,[41] along with Hückel model results for **1** and **2**.

The critical question when comparing the four systems investigated here is why there are such pronounced differences in the spin currents in systems **1** and **2** while there are such minimal changes in systems **3** and **4**. Here, the local transmission can also provide an indication of the underlying cause. Figure 5 illustrates that for structure **4**, the substituted benzene ring, on which most of the spin density is located, essentially does not participate in transport.

The local transmission of **4** is simpler than for **1** and **2**. The pattern corresponds to the one of unsubstituted *meta*-benzene, with an extra ring reversal just slightly above the energy of the peak at −5.05 eV for α electrons, and slightly below the one at −2.00 for β electrons, where small dips in the transmission are visible. This simpler picture is probably due to the two benzene rings being considerably twisted with respect to each other, so that electronic communication is low. The magnitude of this twist may be influenced by the choice of density functional when optimizing the radical structure. Irrespective of the precise magnitude of this effect, as long as the radical substituent is not participating in the transport pathway it is unsurprising that there are no clear spin dependent features in the spin transport.

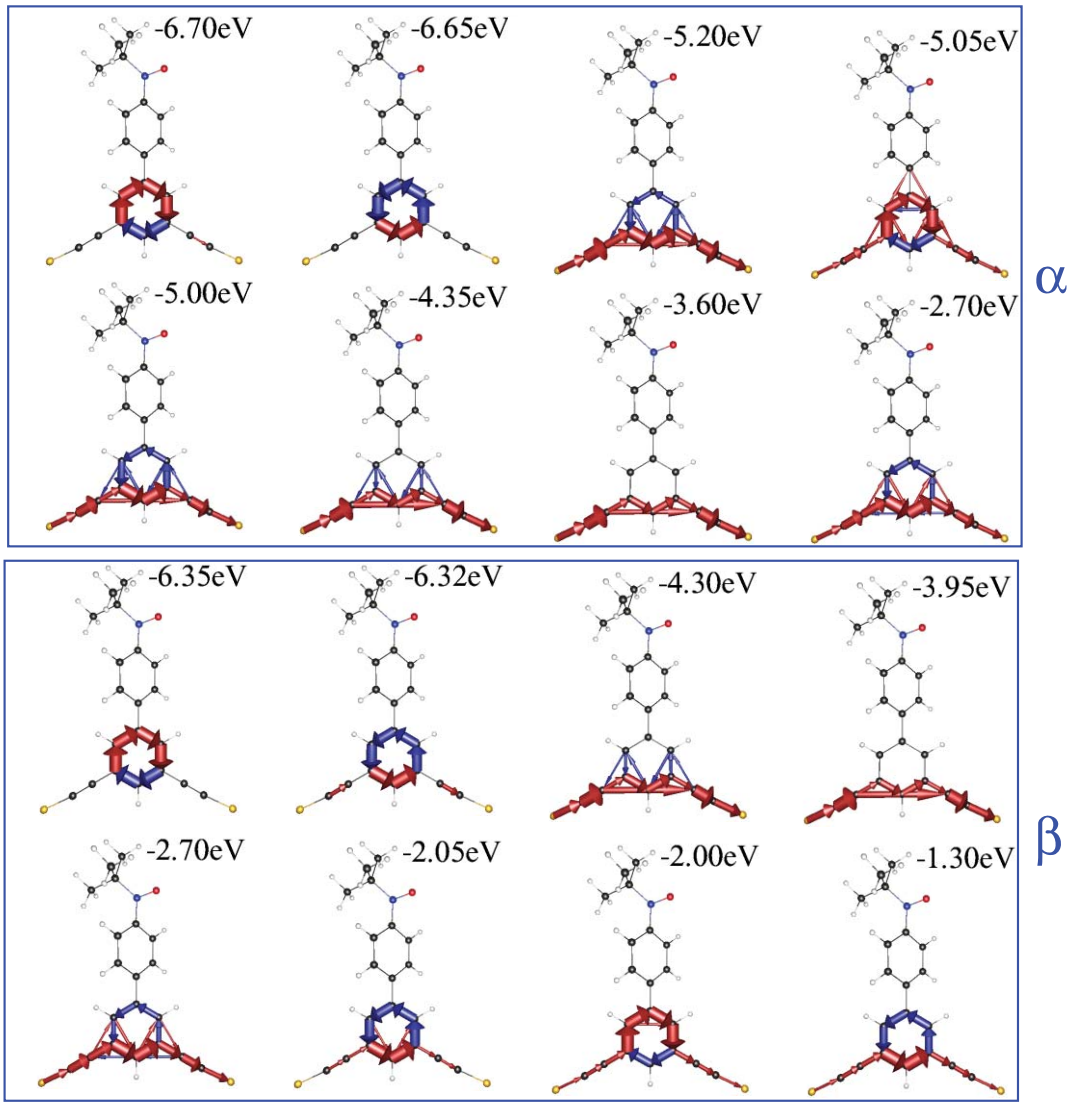

FIG. 5. Representative local transmission plots for system **4**. B3LYP/LANL2DZ. Note that local transmission barely involves the phenylnitroxide substituent on which most of the spin density is located.

V. CONCLUSION AND OUTLOOK

We study which features of the electronic structure make an organic radical a good spin filter for coherent electron transport, provided its (relative) spin orientation can be controlled. We compare two *meta*-connected stable organic radicals, whose electron transfer properties have been studied experimentally,[13,14] to *meta*- and *para*-connected phenoxy model radicals, whose spin-dependent transport properties have been investigated computationally.[24] Our results indicate that spin filtering is large in systems which have a large spin density on the benzene ring attached to the electrodes. This spin density is correlated with large coefficients of the central subsystem HOMO^{α} and LUMO^{β} on the ring atoms, which in turn tends to favor stronger coupling between these MOs and the electrodes.

The local transmission analysis shows that direct contributions of the radical substituent to the transport properties may be removed by extensive twisting between the π-system of the benzene ring connected to the electrodes and the π-plane of the radical substituent. In this case, the parts of the molecule with the majority of the spin density are not the parts of the molecule that participate in the transport, and unsurprisingly then there is very little evidence of the molecules' radical character in the transmission.

We expect *meta*-connected phenoxy radicals (and related open-shell systems with large spin density on the ring) to be more conducting than their closed-shell counterparts, whereas *para*-connected ones should be less conducting than the analogous closed-shell systems. In other words, introducing a radical group that participates in the π-electron system is expected to decrease the *para*-/*meta* conductance ratio. This is of course also true for a closed-shell substituent acting as an additional site in the π system.

While the detailed shapes of spin-resolved transmission curves may depend strongly on the density functional (and, to a lesser extent, on the basis set), overall qualitative results such as the ones found here are not affected by this choice.

Our results suggest that putting a phenoxy radical bridge between a donor and acceptor may test the suggestion that very large spin densities on a connecting benzene ring can affect charge separation and recombination rates.[13,14] Theoretical studies suggest that the spin density distribution in phenoxy radicals can be controlled noticeably by substituents,[60] which makes these systems seem even more attractive. Also, while a bare phenoxy radical is highly reactive, it seems that *t*-butyl phenoxy radicals might be sufficiently stable for such experiments.

Our study concentrated on transport within the π plane. This may prove relevant for donor–bridge–acceptor systems and for single-molecule studies in molecular electronics, and possibly also for one-dimensional polymers. For organic spintronic applications employing bulk systems, it may be interesting to look at the spin filtering properties in the direction perpendicular to the π plane.[61] Also, it would be interesting to investigate temperature effects, spin flips, and inelastic scattering contributions, which may affect spin filtering functionality in ways that are beyond the scope of this initial study.

ACKNOWLEDGMENTS

We thank Michael T. Colvin for helpful discussions, and Joe E. Subotnik for a customized version of QCHEM. C.H. gratefully acknowledges funding through a Forschungsstipendium by the Deutsche Forschungsgemeinschaft (DFG). G.C.S. is supported by The Danish Council for Independent Research | Natural Sciences. This material is based upon work supported as part of the ANSER, an Energy Frontier Research Center funded by the U.S. Department of Energy, Office of Science, Office of Basic Energy Sciences under Award Number DE-SC0001059.

APPENDIX: COMPUTATIONAL METHODS

1. Electronic structure calculations

The dithiol molecules were optimized with an overall charge of zero, using a triple-zeta quality basis set with one set of polarization functions (TZVP (Refs. 62 and 63) and the B3LYP density functional,[42,43] employing the QCHEM (Ref. 64) quantum chemistry program package, with a maximum atomic displacement in subsequent optimization steps below 1.2×10^{-3} Å. After optimization, the thiol groups' hydrogen atoms were stripped off, and the structures were placed between two Au_9 clusters with an sulfur–gold distance of 2.48 Å.[65] Au–Au distances were set to their value in extended gold crystals (2.88 Å). A tight criterion of 10^{-8} a.u. for the direct inversion of the iterative subspace error was chosen in all QCHEM calculations, whereas a criterion of 10^{-6} a.u. was chosen for the largest element of the commutator of the Fock matrix and the density matrix in the ADF calculations.

The density matrix was calculated from the MO coefficients in each step of the self-consistent-field (SCF) algorithm, as usually done for closed systems, and not from the lesser Green's function, which would take the open nature of the system into account.[29,30,66] In other words, the nonequilibrium Green's function formalism was not employed in the SCF algorithm. No periodic boundary conditions were assumed. Spin-unrestricted Kohn-Sham density functional theory calculations were performed using a locally modified version of QCHEM, or ADF (Ref. 50) when indicated. Atom-centered basis set of either contracted Gaussian (QCHEM) or Slater type (ADF) of double-zeta quality (LANL2DZ effective core potential (ECP) with matching basis sets as implemented in QCHEM;[44] DZ (Ref. 50)) or triple-zeta quality with one set of polarization functions (TZVP;[62,63] TZP (Ref. 50)) or two sets of polarization functions (TZ2P (Ref. 50)) were employed. All ADF calculations were carried out within the zeroth-order regular approximation to describe scalar relativistic effects, and used a small frozen core, comprising the 1*s* shell of carbon, nitrogen, and oxygen atoms, and the 1*s* through 4*d* shells of gold atoms. Stuttgart ECPs (Ref. 67) were used for the gold atoms in the TZVP calculations. For the transport calculations, either the B3LYP exchange–correlation functional,[42,43] which features 20% of Hartree–Fock exchange, or the pure density functional BP86 (Refs. 68 and 69) were employed.

2. Electron transport calculations

Transmission functions were obtained by postprocessing output from electronic structure calculations on finite-size electrode–molecule–electrode systems, using routines written in our laboratory[70] according to Eq. (2). $\mathbf{\Gamma}_{X,s}$ and $\mathbf{G}^r_{C,s}$ are calculated from the overlap and Fock matrices of a finite-cluster electrode–molecule–electrode system,

$$\mathbf{\Gamma}_{X,s} = -2\mathrm{Im}[(E\mathbf{S}_{XC} - \mathbf{H}_{XC,s})^\dagger \mathbf{g}_{X,s}(E\mathbf{S}_{XC} - \mathbf{H}_{XC,s})], \tag{A1}$$

$$\mathbf{G}^r_{C,s} = \left(E\mathbf{S}_C - \mathbf{H}_{C,s} + i\tfrac{1}{2}\mathbf{\Gamma}_{R,s} + i\tfrac{1}{2}\mathbf{\Gamma}_{L,s}\right)^{-1}. \tag{A2}$$

The Fock and overlap matrices of the electrode–molecule–electrode system are divided into central, left-electrode, and right-electrode regions. $\mathbf{S}_{XC}$ and $\mathbf{H}_{XC,s}$ denote the coupling block of electrode X and molecule in the overlap and Fock matrix, respectively, while the molecule (or "central region") subblocks of these matrices are indicated by the subscript C. The three gold atoms closest to the sulfur atom were included in the central region to avoid ghost transmission.[71]

The Green's function matrices of the isolated electrodes X ($X \in \{L, R\}$) were calculated in the wide-band-limit (WBL) approximation,

$$(\mathbf{g}_X)_{ij} = -i \cdot \pi \cdot \mathrm{LDOS}^{\mathrm{const}} \cdot \delta_{ij}, \tag{A3}$$

i.e., the local density of states (LDOS) was assumed to be independent of the energy, and the same LDOS value of 0.036 eV^{-1}, obtained from the s-band LDOS for bulk gold from DFT calculations[72] was assigned to all basis functions. Although this is a rather crude approximation, it typically works very well for electrode metals such as gold, which feature a comparatively flat LDOS distribution around the Fermi energy (when plotted as a function of energy), and whose conduction properties are dominated by the broad s band. For example, the same qualitative trends were observed for the transmission of an iron complex[20] regardless of whether the electrodes were described in the WBL approximation or with a more sophisticated tight-binding model.

Energies were not shifted by the system's Fermi energy. This is because the correct choice of the Fermi energy is not obvious for calculations of the type performed here. The Fermi energy of bulk gold (−5.5 eV (Ref. 73)) may be regarded as a rough approximation, although the fact that in practical calculations metal clusters of finite size are used to model the bulk electrodes may shift this value.

Local transmission values between atoms A and B, T_{AB}, were calculated according to[38–40]

$$T_{AB} = \sum_{\mu\in A,\nu\in B} H_{\mu\nu}\mathrm{Im}(\mathbf{G}^r\mathbf{\Gamma}^L\mathbf{G}^a)_{\nu\mu}, \tag{A4}$$

where μ and ν denote the largely atom-centered basis functions which are obtained after carrying out a symmetric (Löwdin) orthogonalization in the central subsystem.

MOs and spin densities were plotted using MOLDEN,[74] with isodensity values of 0.03.

[1] I. Žutić, J. Fabian, and S. D. Sarma, Rev. Mod. Phys. **76**, 323 (2004).
[2] S. A. Wolf, A. Y. Chtchelkanova, and D. M. Treger, IBM J. Res. Dev. **50**, 101 (2006).
[3] P. Seneor, A. Bernand-Mantel, and F. Petroff, J. Phys.: Condens. Matter **19**, 165222 (2007).
[4] W. J. M. Naber, S. Faez, and W. G. van der Wiel, J. Phys. D: Appl. Phys. **40**, R205 (2007).
[5] V. A. Dediu, L. E. Hueso, I. Bergenti, and C. Taliani, Nature Mater. **8**, 707 (2009).
[6] S. Sanvito, J. Mater. Chem. **17**, 4455 (2007).
[7] G. Hu, Y. Guo, J. Wei, and S. Xie, Phys. Rev. B **75**, 165321 (2007).
[8] S. Sanvito, Nature Mater. **6**, 803 (2007).
[9] J. M. Manriquez, G. T. Yee, R. S. McLean, A. J. Epstein, and J. S. Miller, Science **252**, 1415 (1991).
[10] T. Kaneko, T. Matsubara, and T. Aoki, Chem. Mater. **14**, 3898 (2002).
[11] A. Rajca, J. Wongsriratanakul, and S. Rajca, Science **294**, 1503 (2001).
[12] T. Sugawara, M. Minamoto, M. M. Matsushita, P. Nickels, and S. Komiyama, Phys. Rev. B **77**, 235316 (2008).
[13] E. T. Chernick, Q. Mi, R. F. Kelley, E. A. Weiss, B. A. Jones, T. J. Marks, M. A. Ratner, and M. R. Wasielewski, J. Am. Chem. Soc. **128**, 4356 (2006).
[14] E. T. Chernick, Q. Mi, A. M. Vega, J. V. Lockard, M. A. Ratner, and M. R. Wasielewski, J. Phys. Chem. B **111**, 6728 (2007).
[15] R. Landauer, IBM J. Res. Dev. **1**, 223 (1957).
[16] M. Büttiker, Y. Imry, R. Landauer, and S. Pinhas, Phys. Rev. B **31**, 6207 (1985).
[17] G. D. Mahan, *Many-particle Physics* (Plenum, New York, 1990).
[18] R. G. Parr and W. Yang, *Density-Functional Theory of Atoms and Molecules*, vol. 16 of International Series of Monographs on Chemistry (Oxford Science Publications, New York, 1989).
[19] K. Tagami and M. Tsukada, J. Phys. Chem. B **108**, 6441 (2004).
[20] Y. Chen, A. Prociuk, T. Perrine, and B. D. Dunietz, Phys. Rev. B **74**, 245320 (2006).
[21] T. M. Perrine and B. D. Dunietz, J. Phys. Chem. A **112**, 2043 (2008).
[22] R. Liu, S.-H. Ke, W. Yang, and H. U. Baranger, J. Chem. Phys. **127**, 141104 (2007).
[23] R. Liu, S.-H. Ke, H. U. Baranger, and W. Yang, Nano Lett. **5**, 1959 (2005).
[24] C. Herrmann, G. C. Solomon, and M. A. Ratner, J. Am. Chem. Soc. **132**, 3682 (2010).
[25] H.-H. Fu and K.-L. Yao, J. Chem. Phys. **134**, 054903 (2011).
[26] S. Sen and S. Chakrabarti, J. Am. Chem. Soc. **132**, 15334 (2010).
[27] M. Smeu and G. A. DiLabio, J. Phys. Chem. C. **114**, 17874 (2010).
[28] F. A. Carey and R. J. Sundberg, *Advanced Organic Chemistry — Part A: Structure and Mechanisms*, 5th ed. (Springer, New York, 2007).
[29] A. R. Rocha, V. M. García-Suárez, S. Bailey, C. Lambert, J. Ferrer, and S. Sanvito, Phys. Rev. B **73**, 085414 (2006).
[30] Y. Xue, S. Datta, and M. A. Ratner, Chem. Phys. **281**, 151 (2002).
[31] J. Taylor, H. Guo, and J. Wang, Phys. Rev. B **63**, 245407 (2001).
[32] F. Pauly, J. K. Viljas, J. C. Cuevas, and G. Schön, Phys. Rev. B **77**, 155312 (2008).
[33] M. Koentopp, C. Chang, K. Burke, and R. Car, J. Phys.: Condens. Matter **20**, 083203 (2008).
[34] G. C. Liang, A. W. Ghosh, M. Paulsson, and S. Datta, Phys. Rev. B **69**, 115302 (2004).
[35] V. Mujica, A. E. Roitberg, and M. Ratner, J. Chem. Phys. **112**, 6834 (2000).
[36] C. Caroli, R. Combescot, P. Nozieres, and D. Saint-James, J. Phys. C: Solid State Phys. **4**, 916 (1971).
[37] Y. Meir and N. S. Wingreen, Phys. Rev. Lett. **68**, 2512 (1992).
[38] T. N. Todorov, J. Phys.: Condens. Matter **14**, 3049 (2002).
[39] A. Pecchia and A. D. Carlo, Rep. Prog. Phys. **67**, 1497 (2004).
[40] G. C. Solomon, C. Herrmann, T. Hansen, V. Mujica, and M. A. Ratner, Nat. Chem. **2**, 223 (2010).
[41] See supplementary material at http://dx.doi.org/10.1063/1.3598519 for additional data and plots on central subsystem molecular orbitals, parameter dependence, and local transmission.
[42] A. D. Becke, J. Chem. Phys. **98**, 5648 (1993).
[43] C. Lee, W. Yang, and R. G. Parr, Phys. Rev. B **37**, 785 (1988).
[44] P. J. Hay and W. R. Wadt, J. Phys. Chem. **82**, 270 (1985).
[45] Y. Xue, S. Datta, and M. A. Ratner, J. Chem. Phys. **115**, 4292 (2001).
[46] A. Nitzan, Annu. Rev. Phys. Chem. **52**, 681 (2001).
[47] M. Ernzerhof, J. Chem. Phys. **127**, 204709 (2007).
[48] F. Goyer, M. Ernzerhof, and M. Zhuang, J. Chem. Phys. **126**, 144104 (2007).

[49]Y. Shao, L. Fusti-Molnar, Y. Jung, J. Kussmann, C. Ochsenfeld, S. T. Brown, A. T. B. Gilbert, L. V. Slipchenko, S. V. Levchenko, D. P. O'Neill, R. A. Distasio, Jr., R. C. Lochan, T. Wang, G. J. O. Beran, N. A. Besley, J. M. Herbert, C. Y. Lin, T. Van Voorhis, S. H. Chien, A. Sodt, R. P. Steele, V. A. Rassolov, P. E. Maslen, P. P. Korambath, R. D. Adamson, B. Austin, J. Baker, E. F. C. Byrd, H. Dachsel, R. J. Doerksen, A. Dreuw, B. D. Dunietz, A. D. Dutoi, T. R. Furlani, S. R. Gwaltney, A. Heyden, S. Hirata, C.-P. Hsu, G. Kedziora, R. Z. Khalliulin, P. Klunzinger, A. M. Lee, M. S. Lee, W. Liang, I. Lotan, N. Nair, B. Peters, E. I. Proynov, P. A. Pieniazek, Y. M. Rhee, J. Ritchie, E. Rosta, C. D. Sherrill, A. C. Simmonett, J. E. Subotnik, H. L. Woodcock III, W. Zhang, A. T. Bell, A. K. Chakraborty, D. M. Chipman, F. J. Keil, A. Warshel, W. J. Hehre, H. F. Schaefer III, J. Kong, A. I. Krylov, P. M. W. Gill, and M. Head-Gordon, Phys. Chem. Chem. Phys. **8**, 3172 (2006). See http://www.q-chem.com.

[50]G. te Velde, F. M. Bickelhaupt, E. J. Baerends, C. Fonseca Guerra, S. J. A. van Gisbergen, J. G. Snijders, and T. J. Ziegler, J. Comput. Chem. **22**, 931 (2001); Amsterdam Density Functional Program; Theoretical Chemistry, Vrije Universiteit Amsterdam. http://www.scm.com.

[51]C. Chang, M. Pelissier, and P. Durand, Phys. Scr. **34**, 394 (1986).

[52]J.-L. Heully, I. Lindgren, E. Lindroth, S. Lundqvist, and A.-M. Mårtensson-Pendrill, J. Phys. B **19**, 2799 (1986).

[53]E. van Lenthe, E. J. Baerends, and J. G. Snijders, J. Chem. Phys. **99**, 4597 (1993).

[54]P. Sautet and C. Joachim, Chem. Phys. Lett. **153**, 511 (1988).

[55]C. Patoux, C. Coudret, J.-P. Launay, C. Joachim, and A. Gourdon, Inorg. Chem. **36**, 5037 (1997).

[56]J. N. Onuchic, D. N. Beratan, J. R. Winkler, and H. B. Gray, Ann. Rev. Biophys. Biomol. Struct. **21**, 349 (1992).

[57]S.-H. Ke, W. Yang, and H. U. Baranger, Nano Lett. **8**, 3257 (2008).

[58]G. C. Solomon, D. Q. Andrews, T. Hansen, R. H. Goldsmith, M. R. Wasielewski, R. P. Van Duyne, and M. A. Ratner, J. Chem. Phys. **129**, 054701 (2008).

[59]M. Ernzerhof, H. Bahmann, F. Goyer, M. Zhuang, and P. Rocheleau, J. Chem. Theory Comput. **2**, 1291 (2006).

[60]R. J. Fehir, Jr. and J. K. McCusker, J. Phys. Chem. A **113**, 9249 (2009).

[61]G. C. Solomon, C. Herrmann, J. Vura-Weis, M. R. Wasielewski, and M. A. Ratner, J. Am. Chem. Soc. **132**, 7887 (2010).

[62]A. Schäfer, H. Horn, and R. Ahlrichs, J. Chem. Phys. **97**, 2571 (1992).

[63]A. Schäfer, C. Huber, and R. Ahlrichs, J. Chem. Phys. **100**, 5829 (1994).

[64]L. Y. Shao *et al.*, Phys. Chem. Chem. Phys. **8**, 3172 (2006); http://www.q-chem.com.

[65]A. Bilić, J. R. Reimers, and N. S. Hush, J. Chem. Phys. **122**, 094708 (2005).

[66]A. Arnold, F. Weigend, and F. Evers, J. Chem. Phys. **126**, 174101 (2007).

[67]D. Andrae, U. Häussermann, M. Dolg, H. Stoll, and H. Preuss, Theor. Chim. Acta **77**, 123 (1990).

[68]A. D. Becke, Phys. Rev. A **38**, 3098 (1988).

[69]J. P. Perdew, Phys. Rev. B **33**, 8822 (1986).

[70]C. Herrmann and G. C. Solomon, ARTAIOS — a transport code for post-processing quantum chemical electronic structure calculations.

[71]C. Herrmann, G. C. Solomon, J. E. Subotnik, V. Mujica, and M. A. Ratner, J. Chem. Phys **132**, 024103 (2010).

[72]D. A. Papaconstantopoulos, *Handbook of the Band Structure of Elemental Solids* (Plenum, New York, 1986).

[73]N. W. Ashcroft and N. D. Mermin, *Solid State Physics* (Holt Rinehart & Winston, Austin, 1976).

[74]G. Schaftenaar and J. Noordik, J. Comput. Aided Mol. Des. **14**, 123 (2000); http://www.cmbi.ru.nl/molden/molden.html.